https://doi.org/10.5194/egusphere-2026-2401
Preprint. Discussion started: 27 May 2026

Heterogeneous Nitrosation Reactions of Amines Driven by Dinitrogen Tetroxide: A Missing Source of Particulate Nitrosamines

Tai-Xing Chi[1,★], An Ning[2,★], Shuang Ni[1], Wei-Kang Xiao[2], Yang Liu[2], Xiu-Cong Deng[2], Ling Liu[2], Feng-Yang Bai[1,2,*], Zhen Zhao[1,3], and Xiu-Hui Zhang[2,*]

[1]Institute of Catalysis for Energy and Environment, College of Chemistry and Chemical Engineering, Shenyang Normal University, Shenyang 110034, China
[2]State Key Laboratory of Environment Characteristics and Effects for Near-space, Key Laboratory of Cluster Science, Ministry of Education of China, School of Chemistry and Chemical Engineering, Beijing Institute of Technology, Beijing 100081, China
[3]State Key Laboratory of Heavy Oil Processing, China University of Petroleum, Chang Ping, Beijing 102249, China

★These authors contributed equally to this work.

Correspondence to: Feng-Yang Bai (baify492@nenu.edu.cn) and Xiu-Hui Zhang (zhangxiuhui@bit.edu.cn)

ABSTRACT: Nitrosamines are highly carcinogenic and reactive nitrogen-containing pollutants that are widely detected in atmospheric particulate matter; however, their formation mechanisms remain poorly understood. Herein, we elucidate previously unrecognized yet kinetically viable heterogeneous mechanisms for nitrosamine formation via amine-mediated reactions with dinitrogen tetroxide (N_2O_4) at the air–water interface, using Born–Oppenheimer molecular dynamics simulations. The reactions proceed via two distinct pathways: (*i*) barrierless N-nitrosation of methylamine (MA) or dimethylamine (DMA) by N_2O_4, directly yielding nitrosamine cations and nitrate ions (NO_3^-); and (*ii*) MA/DMA-mediated hydrolysis of N_2O_4 produces interfacial HONO rapidly within ~2–16 ps, which can further react with amines to form nitrosamines, albeit with a relatively high reaction barrier of 7.65 kcal mol^{-1}. Overall, the amine-mediated interfacial N-nitrosation reactions proceed rapidly and may represent an important source of particulate nitrosamines. Meanwhile, amine-mediated interfacial hydrolysis of N_2O_4 is a potential source of HONO, proceeding through the combined effects of interfacial water bridging and strong basicity of amines. Our findings reveal a previously overlooked role of heterogeneous interfacial chemistry in elevated particulate nitrosamine formation and coupled HONO production, with important implications for urban reactive nitrogen cycling and its representation in chemical transport models.

1 Introduction

Organic nitrogen (ON) compounds constitute a pivotal yet chemically complex fraction of the global nitrogen cycle, accounting for ~30% of total atmospheric nitrogen (Cape et al., 2011). Active ON precursors play a critical role in atmospheric particle formation, with direct impacts on radiative forcing, regional climate, and public health (Finlayson-Pitts and Pitts Jr, 1999; Seinfeld and Pandis, 2016; Zhang and Anastasio, 2001). Among ON species, nitrosamines containing the

https://doi.org/10.5194/egusphere-2026-2401
Preprint. Discussion started: 27 May 2026

N–NO functional group are of particular concern due to potent carcinogenicity and widespread detection in ambient particles (IARC, 1978). Nitrosamines such as N-nitrosomethylamine (NMA) and N-nitrosodimethylamine (NDMA), which are derived from methylamine (MA) and dimethylamine (DMA) (Choi et al., 2021; Da Silva, 2013), have attracted growing attention in atmospheric chemistry and environmental health research. Notably, particulate NDMA has been detected at considerable levels (up to 20.35 ng m^{-3}) in major urban areas across Asia and Europe, including Seoul, Beijing, Urumqi, London, and Zonguldak (Akyüz and Akyüz, 2025; Choi et al., 2020, 2021, 2025a, b; Farren et al., 2015; Kim et al., 2025; Ma et al., 2025; Wang et al., 2023). However, the formation mechanisms of particulate nitrosamines remain poorly understood (Wang et al., 2023), limiting accurate source apportionment and effective control strategies.

Atmospheric particulate nitrosamines stem from anthropogenic primary emissions, such as vehicular exhaust, fossil-fuel or biomass combustion, and industrial operations (Ge et al., 2011; Nielsen et al., 2012a, b; NTP, 2016). However, increasing evidence also indicates that secondary formation via chemical reactions can contribute substantially to the ambient levels (Choi et al., 2020, 2021), yet all known pathways fail to explain observations. For instance, the gas-phase pathway involving reactions between amine radicals and NO followed by particle partitioning appears insufficient to explain observed nitrosamine levels, as nitrosamines undergo rapid atmospheric photolysis (Nielsen et al., 2012a, b). Furthermore, aqueous-phase ozonation of amines has also been explored (Choi et al., 2024; Karl, 2012a; Mai and Kim, 2024), but this pathway only proceeds under high ozone concentrations that are unrealistic under typical atmospheric conditions. Although amines can undergo aqueous N-nitrosation with N_2O_3/N_2O_4/HONO (Challis and Kyrtopoulos, 1979; Choi et al., 2021, 2025a; Hutchings et al., 2010; Karl, 2012b), the predicted reaction rates of these aqueous-phase processes are too slow to account for the high measured concentrations (Choi et al., 2021; Karl, 2012b), strongly suggesting a critical yet unrecognized source of particulate nitrosamines.

Given the limitations of the gas- and aqueous-phase pathways, combined with the evident interfacial propensity of MA and DMA (Deng et al., 2026; Ning et al., 2023, 2024) and the known reaction-accelerating effect of the air–water interface (Fang et al., 2025; Song et al., 2024), we infer that heterogeneous interfacial chemistry is a potential source of nitrosamines. Meanwhile, N_2O_4—a critical nitrosamine precursor—has been shown to reside at the air–water interface for ~100 ps before dissolving into the bulk liquid (Martins-Costa et al., 2020). Thus, these gaseous species (MA, DMA, and N_2O_4) can adsorb at the interface, rendering interfacial reactions likely feasible. Although this interfacial process could represent a previously unrecognized nitrosamine source, its kinetic feasibility and molecular mechanism remain unexplored.

In this work, we systematically investigate the heterogeneous reaction pathways of MA and DMA with N_2O_4 at the air–water interface to identify whether this mechanism explain the high particulate nitrosamine levels observed in polluted regions. Through Born–Oppenheimer molecular dynamics (BOMD) and well-tempered metadynamics (MetaD) simulations, we map the reaction free energy landscapes at an ambient temperature (T = 300 K). Our simulations elucidate the heterogeneous formation mechanism of nitrosamines and clarify the roles of amine basicity, water-bridged proton transfer, and steric hindrance in the reaction, thereby providing molecular-level insights into this potential atmospheric formation pathway.

https://doi.org/10.5194/egusphere-2026-2401
Preprint. Discussion started: 27 May 2026

2 Computational Methods

2.1 Born−Oppenheimer molecular dynamics (BOMD) Simulations

The heterogeneous reaction mechanisms at the air–water interface were investigated using BOMD simulations, with enhanced sampling achieved via well-tempered metadynamics (MetaD). All simulations were performed using the CP2K 2023 software interfaced with the PLUMED 2.9.0 plugin (Bussi and Tribello, 2019; Kühne et al., 2020). The calculations of electronic structure were carried out by the QUICKSTEP module, with the Gaussian and plane wave (GPW) method and the Becke–Lee–Yang–Parr (BLYP) exchange–correlation functional (Perdew and Wang, 1992), which was supplemented with the Grimme's D3 dispersion correction. And the DZVP-MOLOPT-SR-GTH Gaussian basis set and Goedecker–Teter–Hutter (GTH) pseudopotentials were employed to describe the valence and core electrons, respectively (Goedecker et al., 1996; Hartwigsen, 1998). The energy cutoff for the Gaussian basis set was set to 40 Ry, while that for plane-wave basis set was 280 Ry. The *NVT* ensemble was employed, with a time step of 1.0 fs. The Nosé–Hoover thermostat (Evans and Holian, 1985) was adopted to control a constant temperature of 300 K. The simulated cell (15 Å × 15 Å × 45 Å) contained 128 water molecules, with the air–water interface defined by a vacuum region (~30 Å) above the water slab (~15 Å) along the *Z* direction (Fig. S1). The water slab was equilibrated for 10 ps using BOMD simulations, and the temperature and potential energy profiles confirming the achievement of statistical equilibrium (Fig. S2). The details of the collective variable (CV) are provided in the Supporting Information.

2.2 Quantum Chemical Calculations

To obtain the potential energy surfaces for the gas- and aqueous-phase reactions between HONO and DMA, quantum chemical calculations were performed. All stationary points and transition states were optimized using the B3LYP-D3 (Becke, 1993; Lee et al., 1988) functional with the 6-311++G(3df,2p) basis set as implemented in the Gaussian 16 package (Frisch et al., 2016). This level of theory has been validated to provide reliable results (Chacón et al., 2020; Li et al., 2018; Wang and Agmon, 2017). Frequency calculations of the optimized structures were performed at the same level of theory, confirming that each transition state possesses a single imaginary frequency, whereas all minima exhibit no imaginary frequencies (Table S1). Moreover, the intrinsic reaction coordinate (IRC) (Hratchian and Schlegel, 2004, 2005) calculations were carried out to confirm that each transition-state structure connects the corresponding reactant and product. Subsequently, the single-point energy was refined at the CCSD(T)/aug-cc-pVTZ level of theory. The aqueous reaction was studied using the SMD (Solvation Model based on Density) implicit solvation model (Marenich et al., 2009), in which water is treated as a polarizable continuum to account for bulk solvent effects.

2.3 Wave Function Analysis

To gain further insights into the interfacial reaction mechanisms, the wave function analysis of key structures was performed using the Multiwfn 3.8 program (Lu and Chen, 2012), while the results were visualized by VMD 1.9.3 (Humphrey et al.,

https://doi.org/10.5194/egusphere-2026-2401
Preprint. Discussion started: 27 May 2026

1996). Specifically, the Mayer bond order (MBO) was calculated to quantify the strength of covalent bonds within the reactant molecules. Interaction Region Indicator (IRI) analysis was carried out to examine the strength of localized interactions in prereactants and the intermolecular noncovalent interactions within interfacial products, such as hydrogen bonds (HBs). The electron localization function (ELF) was applied to probe covalently bonded regions with high ELF values, indicative of strong electron localization.

3 Results

3.1 Interfacial N-nitrosation reactions of MA/DMA with N_2O_4

To elucidate the heterogeneous formation pathways of nitrosamines, the reactions of MA and DMA with N_2O_4 were investigated at the air–water interface using BOMD simulations. Based on the previous studies of interfacial N_2O_4 chemistry, N_2O_4 exists as the symmetric dimer $O_2N–NO_2$, which can isomerize to the asymmetric form *t*-$ONONO_2$ (Finlayson-Pitts et al., 2003; Martins-Costa et al., 2019, 2020). Thus, *t*-$ONONO_2$ was used as the reactant to explore the heterogeneous N-nitrosation mechanisms between N_2O_4 and amines. In a three-component system consisting of *t*-$ONONO_2$, the amines (MA/DMA), and interfacial water, any two species can collide and react at the air–water interface. Three collision modes between MA/DMA and *t*-$ONONO_2$ on aqueous nanodroplet surfaces were examined (Scheme 1). Mode (*i*) corresponds to gaseous MA/DMA approaching *t*-$ONONO_2$ pre-adsorbed on aqueous aerosol droplet surface. Mode (*ii*) describes a gaseous MA/DMA–*t*-$ONONO_2$ complex colliding with the aqueous interface. Mode (*iii*) involves gaseous *t*-$ONONO_2$ approaching MA/DMA pre-adsorbed on the water surface.

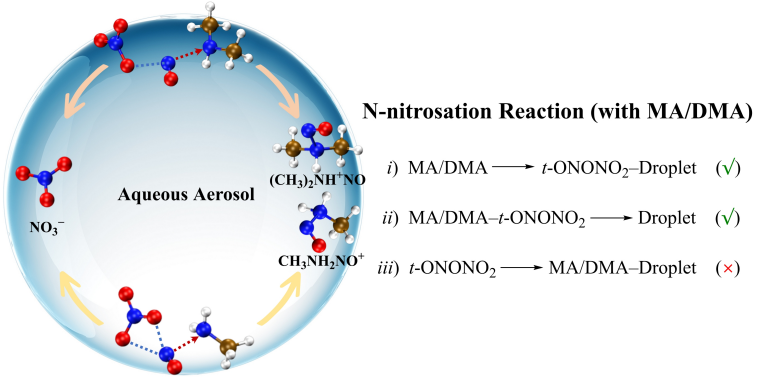

Scheme 1. Illustration of the interfacial N-nitrosation mechanism of MA/DMA initiated by *t*-$ONONO_2$ (MA/DMA + *t*-$ONONO_2$ → $CH_3NH_2NO^+$/$(CH_3)_2NH^+NO$ + NO_3^-. The dashed lines denote ionic bond (blue), whereas the arrows indicate the formation of $CH_3NH_2NO^+$/$(CH_3)_2NH^+NO$ (red). Patterns *i*)–*iii*) illustrate different collision scenarios, with black arrows showing the directions of collision. The blue, red, white, and ochre spheres represent the N, O, H, and C atoms, respectively. The symbols "√" and "×" denote whether the reaction can or cannot occur, respectively.

https://doi.org/10.5194/egusphere-2026-2401
Preprint. Discussion started: 27 May 2026

Figure 1 corresponds to mode (*i*) in Scheme 1. Initially, *t*-$ONONO_2$ was placed at the air–water interface and equilibrated for 15 ps. Analyses of temperature and potential energy confirmed that statistical equilibrium was reached at 11.5 ps (Fig. S3). This equilibrated structure was used as the initial configuration. Notably, *t*-$ONONO_2$ underwent spontaneous heterolysis to form a stable $(NO_3^-)(NO^+)$ ion pair at the interface by 11.5 ps, which is consistent with previous interfacial simulations by Martins-Costa et al (2020). For the MA-involved reaction (Fig. 1(a)), MA was initially in the gas phase at t = 0 ps with negligible interactions with the aqueous surface. It rapidly approached the interfacial NO^+ ion, and by 0.99 ps, the N2 atom of MA and N1 atom of NO^+ formed a N1–N2 bond, yielding the cationic nitrosamine *c*-$CH_3NH_2NO^+$. To further understand the N-nitrosation process of *t*-$ONONO_2$ with MA, electron localization function (ELF) analysis was performed for key structures. As shown in Fig. 1(b), strong electron localization within the newly formed N1–N2 bond confirms the formation of the nitrosamine and nitrate ions. Extended BOMD simulations up to 21 ps verified that the products *c*-$CH_3NH_2NO^+$ and NO_3^- remained stable at the air–water interface (Fig. 1(c)). Identical reactions from different initial conformations further support the robustness of this pathway (Fig. S4).

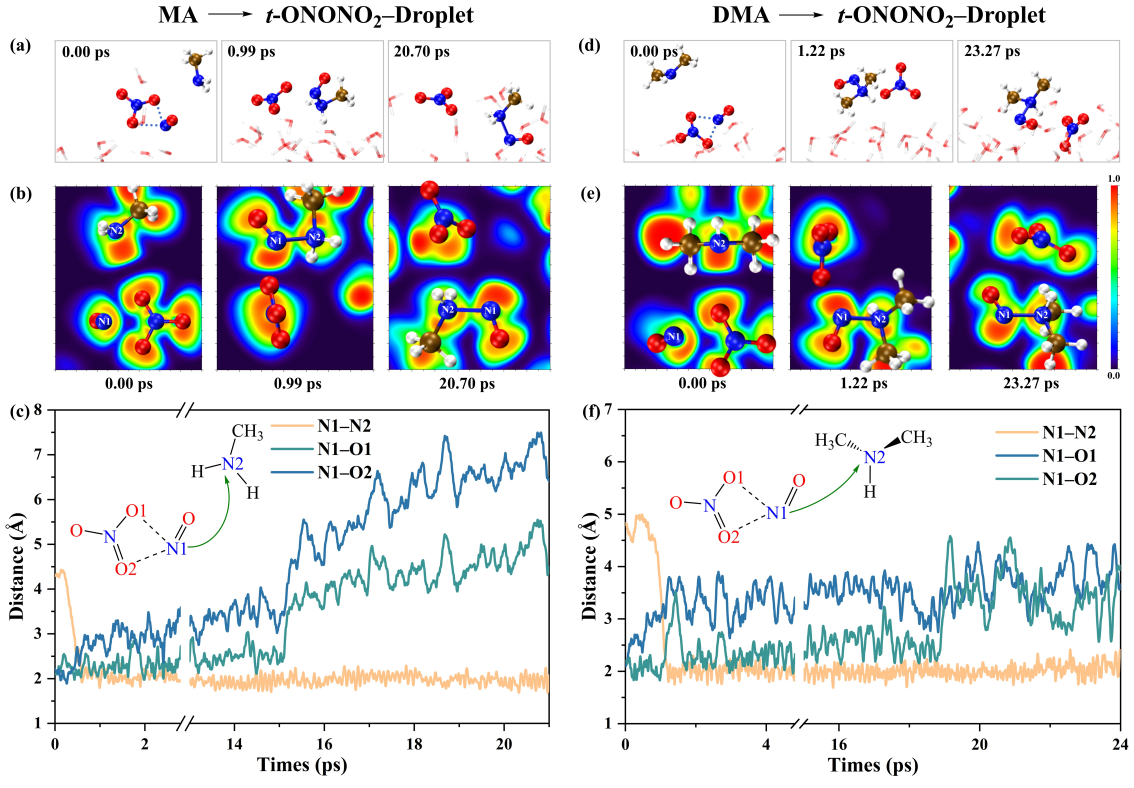

Figure 1. Snapshot structures from BOMD simulations illustrating the stepwise N-nitrosation mechanism of *t*-$ONONO_2$, color-mapped electron localization function (ELF), and the time evolution of key bond distances mediated by MA **(a, b, c)** and DMA **(d, e, f)**. The black arrows indicate the directions of collision, while the dashed lines represent ionic bond. The blue, red, white, and ochre spheres represent the N, O, H, and C atoms, respectively. The green arrows denote atom transfer directions.

https://doi.org/10.5194/egusphere-2026-2401
Preprint. Discussion started: 27 May 2026

As shown in Fig. 1(d), the DMA-mediated formation of $(CH_3)_2NHNO^+$ follows the same mechanism as MA. In both MA and DMA systems, nitrosamine cations form within ~1 ps and remain stable at the interface throughout the simulations. Moreover, mode (*ii*) (Scheme 1) was also verified to be reactive. As shown in Fig. S5, the gaseous MA/DMA–*t*-$ONONO_2$ complex undergoes rapid N-nitrosation upon contacting the air–water interface, forming nitrosamine cations within 0.85 ps (MA) and 0.33 ps (DMA). These products also remain stable at the interface. Notably, mode (*iii*) did not yield direct N-nitrosation in any simulation. After equilibration, the N atom of MA/DMA formed hydrogen bonds with interfacial water, blocking the nucleophilic nitrogen site and inhibiting N-nitrosation. Interestingly, although mode (*iii*) does not produce nitrosamines directly, it efficiently promotes amine-mediated hydrolysis of *t*-$ONONO_2$ to generate HONO, protonated amine, and NO_3^-. Since HONO is also a key nitrosamine precursor, this pathway is explored in detail in the next section.

3.2 MA- and DMA-Mediated Interfacial Hydrolysis of *t*-$ONONO_2$

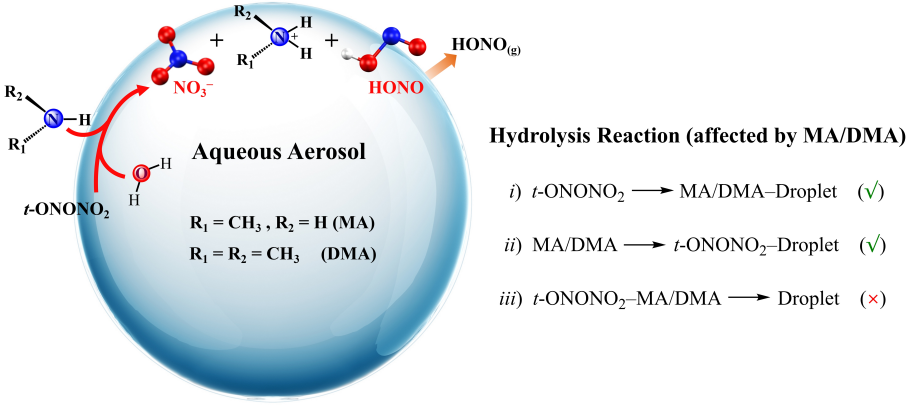

Scheme 2. Illustration of the interfacial mechanism of *t*-$ONONO_2$ hydrolysis affected by MA/DMA (*t*-$ONONO_2$ + MA/DMA + H_2O → HONO + NO_3^- + MAH^+/$DMAH^+$). Patterns *i*)–*iii*) illustrate different collision scenarios, with the black arrows indicating the directions of collision. The symbols "√" and "×" denote whether the reaction can or cannot occur, respectively.

We further explored the role of amines in the heterogeneous hydrolysis of *t*-$ONONO_2$. Three collision modes at the aqueous aerosol surface were investigated (Scheme 2): (*i*) gaseous *t*-$ONONO_2$ colliding with pre-adsorbed MA/DMA; (*ii*) gaseous MA/DMA approaching pre-adsorbed *t*-$ONONO_2$; (*iii*) gaseous MA/DMA–*t*-$ONONO_2$ complexes adsorbing onto the water surface.

Key structures and bond-length evolutions for MA- and DMA-mediated hydrolysis corresponding to mode (*i*) are presented in Figs. 2(a)–2(d). MA was initially positioned above the water slab and equilibrated for 10 ps. Temperature and potential energy profiles confirmed equilibrium within 10 ps (Fig. S6). At equilibrium, the N atom of MA formed a hydrogen bond (HB) with interfacial water. As shown in Fig. 2(a), gaseous *t*-$ONONO_2$ does not interact with interfacial water (t = 0 ps). As the simulation proceeds, *t*-$ONONO_2$ approaches the interface and rapidly dissociates into an $(NO_3^-)(NO^+)$ ion pair, consistent with previous reports (Martins-Costa et al., 2020) showing that this ion pair forms on the femtosecond

https://doi.org/10.5194/egusphere-2026-2401
Preprint. Discussion started: 27 May 2026

scale and remains stable for ~100 ps at the air–water interface. Mayer bond order (MBO) and Interaction Region Indicator (IRI) analyses (Figs. S7, S8) revealed that the N2–O3 bond was the weakest, supporting this dissociation pathway. A pre-reaction complex formed at 7.54 ps, in which interfacial water bridged the (NO_3^-)(NO^+) ion pair and MA via H1–O2···N1 and O2–H1···N2 hydrogen bonds (Fig. 2(b)). Subsequently, proton H1 transfers from H_2O to MA at 8.40 ps. The resulting OH^- then attacked the N1 atom of the NO^+ ion, forming a new covalent N1–O2 bond and generating HONO by 8.48 ps. The final products are HONO, NO_3^-, and MAH^+.

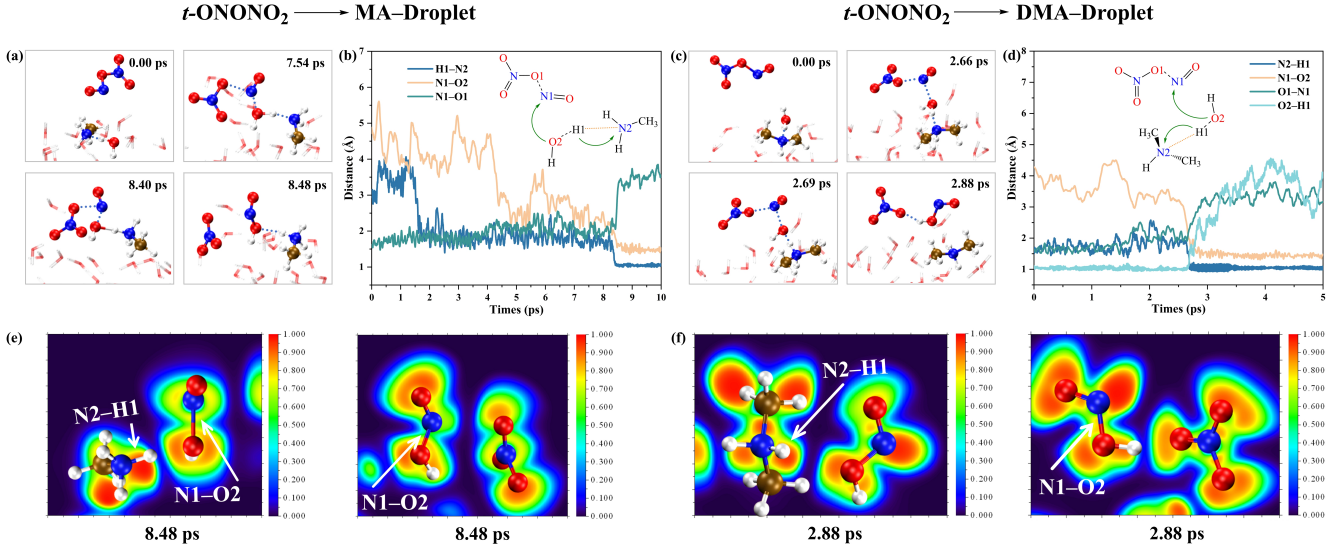

Figure 2. Snapshot structures from BOMD simulations depicting the stepwise mechanism and the time evolution of key bond distances for the hydrolysis reaction of *t*-$ONONO_2$ mediated by MA **(a, b)** and DMA **(c, d)**. Color-mapped ELF for the products of MA- and DMA-mediated hydrolysis of *t*-$ONONO_2$, respectively: **(e)** HONO, MAH^+, and NO_3^- (8.48 ps); **(f)** HONO, $DMAH^+$, and NO_3^- (2.88 ps). The black arrows indicate the directions of collision, while the dashed lines represent intermolecular interactions (ionic bond and hydrogen bond). The blue, red, white, and ochre spheres represent the N, O, H, and C atoms, respectively. The green arrows denote atom transfer directions.

Similar to MA, DMA also initially formed a hydrogen bond with interfacial water (Fig. S9) and mediated *t*-$ONONO_2$ hydrolysis via an identical mechanism but on a shorter timescale (2.88 ps), ultimately yielding HONO, NO_3^-, and $DMAH^+$ (Figs. 2(c, d)). The faster kinetics can be attributed to the stronger basicity of DMA relative to MA, which promotes more efficient proton transfer and accelerates bond cleavage in *t*-$ONONO_2$. Furthermore, ELF analysis of the final structures (Figs. 2(e, f)) confirms clear electron localization in the N1–O2 and N2–H1 covalent bonds, as well as fully separated HONO, MAH^+, $DMAH^+$, and NO_3^-. These results demonstrate that *t*-$ONONO_2$ undergoes "single–water" hydrolysis at the aqueous interface, with only one water molecule directly participating.

https://doi.org/10.5194/egusphere-2026-2401
Preprint. Discussion started: 27 May 2026

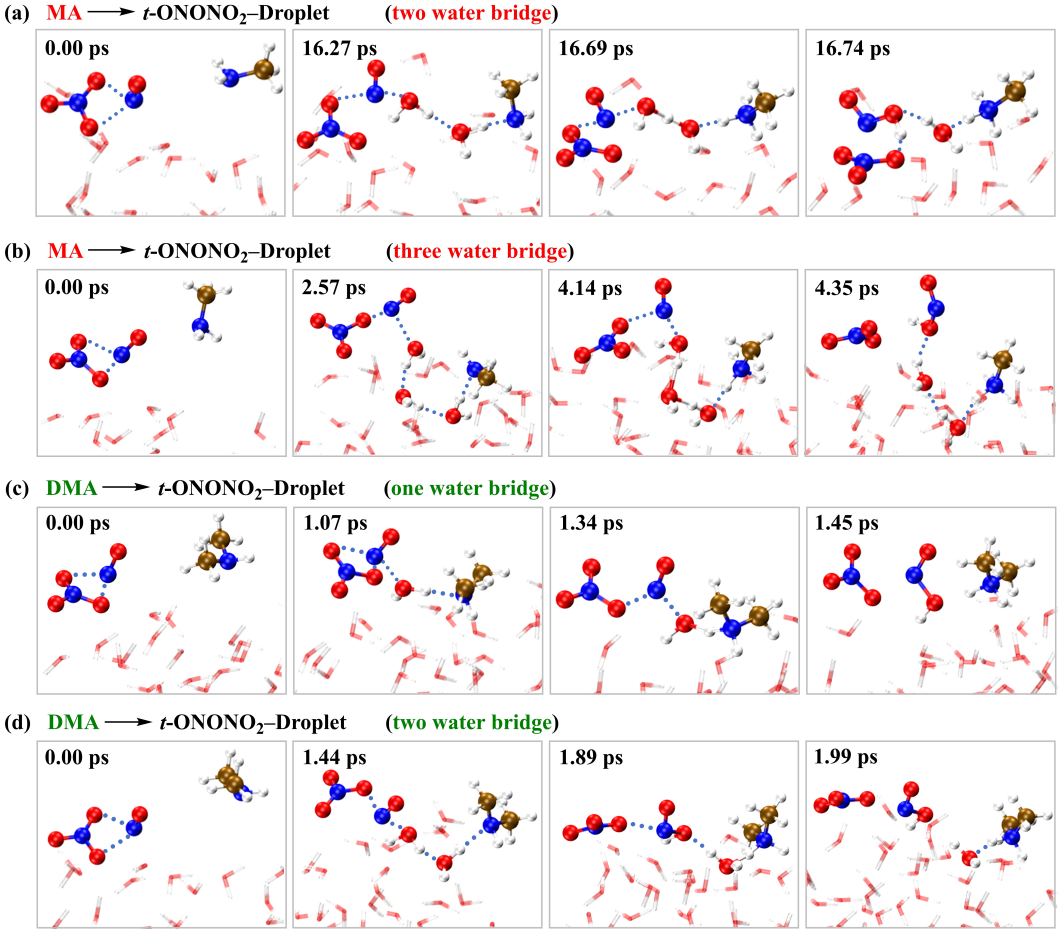

Figure 3. Snapshot structures from the BOMD simulations, illustrating the stepwise mechanism of the **(a, b)** MA- and **(c, d)** DMA-mediated hydrolysis reaction of *t*-$ONONO_2$. The black arrows indicate the directions of collision, while the dashed lines represent intermolecular interactions. The blue, red, white, and ochre spheres represent the N, O, H, and C atoms, respectively.

For mode (*ii*) (Scheme 2), gaseous MA/DMA approaches pre-adsorbed *t*-$ONONO_2$. Key structures and bond evolutions are shown in Figs. 3 and S10. For the MA-involved reactions (Figs. 3(a) and S10(a)), MA initially resides in the gas phase without notable interactions with the interfacial water. By 16.27 ps, MA forms an O4–H2···N2 HB with H_2O. Concurrently, interfacial water connects NO^+ ion and MA via a two-water bridge (O3–H1···O4–H2), forming a pre-reaction complex. At 16.69 ps, the H2 proton transfer from H_2O to MA generates MAH^+ and OH^-, which rapidly moves toward H1 of the proximate water molecule to form another OH^-. At 16.74 ps, O3–N1 bond formation between NO^+ and second OH^- concludes the reaction, producing HONO, NO_3^-, and MAH^+ as the final products. Notably, the catalytic hydrolysis mechanism depends on the contact configuration between gaseous MA and the interface. As shown in Figs. 3(b) and S10(b), the gaseous MA approaches interfacial water, forming the O5–H3···N2 HB at 2.57 ps. Meanwhile, interfacial water connects the NO^+ ion to MA via a three-water bridge (O3–H1···O4–H2···O5–H3), forming a pre-reaction complex. Proton transfer

https://doi.org/10.5194/egusphere-2026-2401
Preprint. Discussion started: 27 May 2026

from water to MA occurs at 4.14 ps, followed by proton relay along the water bridge that produces OH^-. By 4.35 ps, NO^+ reacts with OH^- via O3–N1 bond formation to produce fully separated HONO, NO_3^-, and MAH^+. For MA, a pre-reaction complex forms via two-water or three-water bridges between NO^+ and MA. Proton transfer occurs along the water bridge, followed by OH^- attack on NO^+ to form HONO. Remarkably, the three-water-bridge pathway proceeds approximately four times faster than the two-water-bridge pathway. This kinetic enhancement may stem from the greater stability of the "three-water bridge" structure, whose larger spatial configuration hinders rotation at the water interface, thereby stabilizing its connections with NO^+ and MA at both ends and facilitating proton transfer.

For the DMA-involved reactions (Figs. 3(c, d) and S10(c, d)), the interfacial hydrolysis of *t*-$ONONO_2$ follows the same mechanism but proceeds even more rapidly (~1–2 ps). This acceleration is again attributed to the stronger basicity of DMA, a result consistent with collision mode (*i*). Notably, in MA-mediated hydrolysis, proton transfer through a three-water bridge occurs faster than through a two-water bridge, highlighting the catalytic advantage of increasing the length of interfacial water bridge. In contrast, DMA-mediated hydrolysis exhibits nearly identical reaction times for single- and two-water bridges (~1–2 ps), indicating that additional water molecules provide little further kinetic enhancement. This can be attributed to the stronger basicity of DMA than MA, which enables rapid proton abstraction from interfacial water and facilitates proton transfer, thereby promoting hydrolysis. Overall, MA- and DMA-catalyzed interfacial hydrolysis of *t*-$ONONO_2$ can promote aerosol growth through enhancement of hygroscopicity, owing to the formation of (*i*) nitrate (NO_3^-) and (*ii*) protonated amines (MAH^+ and $DMAH^+$), which substantially increase aerosol water uptake (Deng et al., 2026; Ning et al., 2023, 2024). The MA- and DMA-mediated hydrolysis of *t*-$ONONO_2$ proceeds on the picosecond timescale and efficiently produces HONO. This high HONO yield is governed by the synergistic coupling between interfacial water bridges and amine basicity, which facilitate proton transfer.

Given the high reactivity of HONO, its kinetic behavior warrants investigation at the air–water interface. As shown in Fig. S11, IRI analysis reveals weak noncovalent interactions between HONO and interfacial water, supporting the finding by Chen et al. (Chen et al., 2025) that HONO predominantly exists in its neutral form at the interface of aqueous microdroplets. More importantly, HONO is recognized as a key precursor to N-nitrosodimethylamine (NDMA) (Ge et al., 2011; Karl, 2012b), despite its relatively slow bimolecular reaction rate with dimethylamine (DMA) in the aqueous phase (~0.1 M^{-1} s^{-1}) (Karl, 2012b). However, the heterogeneous reaction mechanism of HONO with DMA at the air–water interface remains poorly understood, yet its elucidation is essential to quantitatively assess their contribution to particulate nitrosamine formation.

3.3 Interfacial Reaction of DMA with HONO

To evaluate whether interfacially generated HONO contributes to nitrosamine formation, the reaction of DMA with HONO at the air–water interface was studied using BOMD and MetaD simulations. As shown in Figs. 4(a, b), HONO first undergoes N–O bond cleavage to form an OH^-/NO^+ ion pair. Concurrently, the N–H bond of DMA dissociates; the released proton (H^+) neutralizes OH^- to form an H_2O molecule, while electrophilic NO^+ attacks $(CH_3)_2N^-$ to yield NDMA. Although

https://doi.org/10.5194/egusphere-2026-2401
Preprint. Discussion started: 27 May 2026

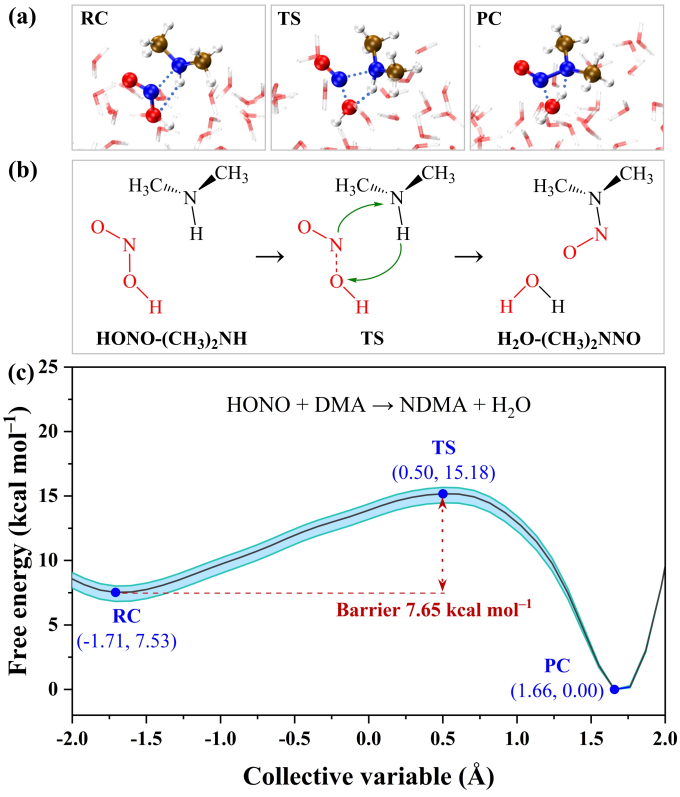

Figure 4. Direct interfacial N-nitrosation of DMA by HONO at the air-water interface. **(a)** Snapshots of the reactant complex (RC), transition state (TS), and product complex (PC) during the WT-MetaD simulations; **(b)** Reaction mechanism for DMA + HONO → NDMA + H_2O. **(c)** Free energy profile along the collective variable (black line) for the N-nitrosation process with the error band (blue region). The dashed lines represent intermolecular interactions, while the green arrows denote atom transfer directions.

the calculated energy barrier for this process is 7.65 kcal mol^{-1} (Fig. 4(c)), which is significantly lower than in the gas phase (27.99 kcal mol^{-1}) and bulk aqueous phase (22.64 kcal mol^{-1}, Fig. S12). Nonetheless, this barrier remains relatively high, indicating that this pathway represents a minor route for NDMA formation at the air–water interface. Using transition state theory (TST), the interfacial rate constant at 300 K is 1.67×10^7 M^{-1} s^{-1}, roughly 7–8 orders of magnitude faster than the reported aqueous-phase value (~0.1 M^{-1} s^{-1}) (Karl, 2012b). Computational details are provided in the Supporting Information (Section S4). Although this pathway is kinetically enhanced relative to bulk processes, it is still less efficient than direct N-nitrosation by N_2O_4. In summary, direct interfacial N-nitrosation of amines by N_2O_4 dominates particulate nitrosamine formation, while HONO-mediated nitrosation plays a secondary role.

4 Conclusion

https://doi.org/10.5194/egusphere-2026-2401
Preprint. Discussion started: 27 May 2026

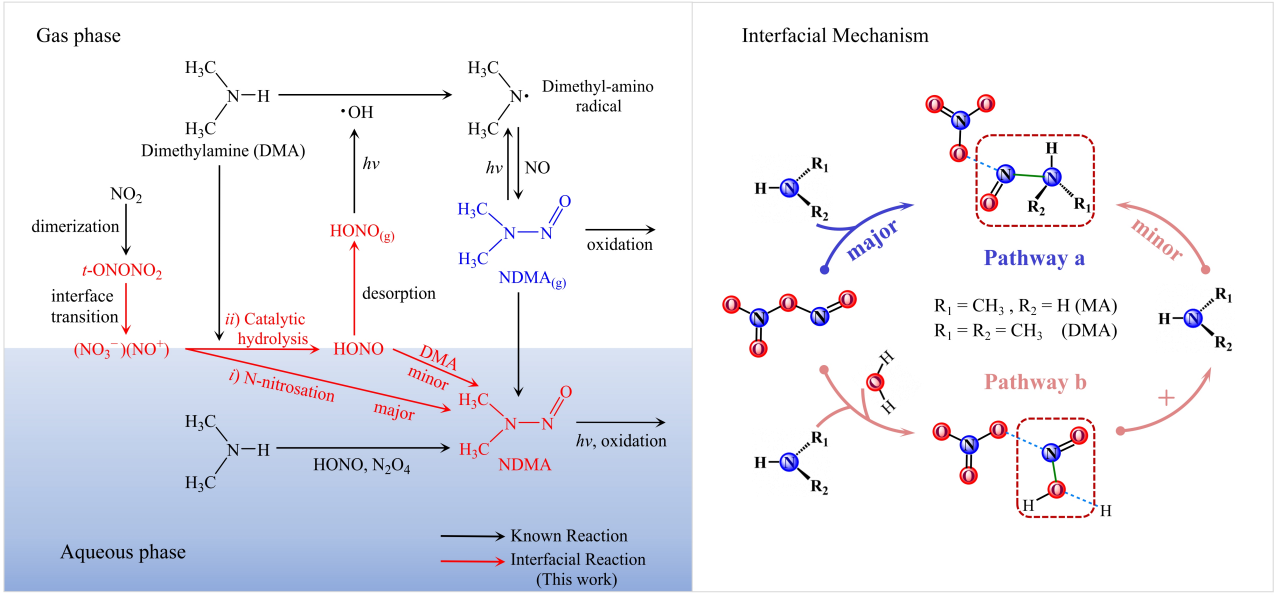

Figure 5. Schematic illustration of simplified reactive nitrogen chemistry. Black arrows represent the established gas-phase or aqueous-phase reaction pathways, whereas red arrows indicate the revealed amine-mediated heterogeneous reactions occurring at the air–water interface of aqueous aerosols. The right panel shows the detailed interfacial reaction pathway.

Particulate nitrosamines are carcinogenic organic nitrogen compounds of growing concern, yet their formation remains poorly understood, which limits accurate assessments of their impacts on air quality, climate, public health, and reactive nitrogen cycling. Particulate nitrosamines have been frequently detected at high concentrations in atmospheric particles across multiple cities in Asia and Europe. However, existing sources cannot fully account for these levels, indicating the presence of missing nitrosamine sources. To investigate these unknown origins, we employed Born-Oppenheimer molecular dynamics (BOMD) and metadynamics (MetaD) simulations to explore the heterogeneous reaction processes of MA/DMA with N_2O_4 (nitrosamine precursors) on aqueous aerosol surfaces. The results demonstrate that the spontaneous direct nitrosation of MA/DMA with N_2O_4 at the air–water interface dominates the formation of particulate-phase nitrosamines. Additionally, MA/DMA can catalyze the spontaneous hydrolysis of N_2O_4 to generate HONO at the air-water interface. The subsequent reaction of HONO with DMA to form the nitrosamine NDMA, by overcoming a free energy barrier of 7.65 kcal mol^{-1}, represents a secondary formation pathway at the interface. Consequently, we identify a critical, previously overlooked heterogeneous pathway at the air–water interface: in the presence of MA or DMA, N_2O_4 is rapidly converted into nitrosamines and HONO. These findings carry important environmental implications: (*i*) the nitrosamines formed at the interface increase the carcinogenic potential of atmospheric particulate matter, thus posing heightened risks to human health; (*ii*) the formed HONO can undergo photolysis to produce ·OH radicals, which can enhance the tropospheric oxidation capacity and promote the formation of secondary pollutants. Meanwhile, these reactions concurrently generate NO_3^-, contributing to the aerosol nitrate burden. Furthermore, the NO released from the photolysis of HONO and nitrosamines can

https://doi.org/10.5194/egusphere-2026-2401
Preprint. Discussion started: 27 May 2026

re-enter the NO_x cycle. By incorporating the revealed interfacial N-nitrosation pathway into the established scheme of gas- and aqueous-phase nitrogen chemistry, this study advances and broadens our current understanding of multiphase reactive nitrogen cycling (Fig. 5). This mechanism provides a consistent molecular explanation for the frequently observed high nitrosamine levels in cloud water, fog, and urban $PM_{2.5}$. Incorporating this heterogeneous interfacial chemistry into atmospheric chemical transport models may improve predictions of particulate toxicity, nitrogen chemistry and budget. More broadly, by converting gaseous reactive nitrogen into particulate nitrogen, these findings underscore the key role of heterogeneous interfacial chemistry in shaping the global nitrogen cycle.

Data availability. The data in this article are available from the corresponding author upon reasonable request (baify492@nenu.edu.cn and zhangxiuhui@bit.edu.cn).

Supplement. The supplement related to this article is available online at:

Author contribution. ★TC and ★AN contributed equally to this work. XZ, ZZ, and FB designed and supervised the research. TC, XD, and AN performed the quantum chemical calculations and the BOMD simulations. TC, AN, SN, WX, YL and LL analyzed data. TC, AN, FB, and XZ wrote the paper with contributions from all the other co-authors.

Competing interests. The contact author has declared that neither they nor their co-authors have any competing interests.

Disclaimer. Publisher's note: Copernicus Publications remains neutral with regard to jurisdictional claims in published maps and institutional affiliations.

Financial support. This work was financially supported by the National Natural Science Foundation of China (No. 22476134 and 22306011), the National Science Foundation for Distinguished Young Scholars (No. 22225607), and the Central Government Guided Local Science and Technology Development Fund (No. 2026JH6/101000020) under the "Free Exploration Program for Young Scientists (Liaoning Provincial Youth B). Feng-Yang Bai was also supported by the China Postdoctoral Science Foundation (No. 2024M754098).

https://doi.org/10.5194/egusphere-2026-2401
Preprint. Discussion started: 27 May 2026

References

Akyüz, B. G. and Akyüz, M.: Seasonal variations, source apportionment, and health risk assessment of nitrosamines in inhalable particulate matter (PM_{10}) in the atmosphere of Zonguldak, Türkiye, Environ. Sci. Pollut. Res., 32, 11083–11096, https://doi.org/10.1007/s11356-025-36280-z, 2025.

Becke, A. D.: Density-functional thermochemistry. III. The role of exact exchange, J. Chem. Phys., 98, 5648–5652, https://doi.org/10.1063/1.464913, 1993.

Bussi, G. and Tribello, G. A.: Analyzing and Biasing Simulations with PLUMED, in: Biomolecular Simulations: Methods and Protocols, edited by: Bonomi, M. and Camilloni, C., Springer, New York, NY, 529–578, https://doi.org/10.1007/978-1-4939-9608-7_21, 2019.

Cape, J. N., Cornell, S. E., Jickells, T. D., and Nemitz, E.: Organic nitrogen in the atmosphere — Where does it come from? A review of sources and methods, Atmos. Res., 102, 30–48, https://doi.org/10.1016/j.atmosres.2011.07.009, 2011.

Chacón, K. N., Espinal, J. F., Montero-Campillo, M. M., Yáñez, M., and Mejía, S. M.: Looking for the Azeotrope: A Computational Study of $(Ethanol)_6$–Water, $(Methanol)_6$–Water, $(Ethanol)_7$, and $(Methanol)_7$ Heptamers, J. Phys. Chem. A, 124, 7080–7087, https://doi.org/10.1021/acs.jpca.0c05362, 2020.

Challis, B. C. and Kyrtopoulos, S. A.: The chemistry of nitrosocompounds. Part 11. Nitrosation of amines by the two-phase interaction of amines in solution with gaseous oxides of nitrogen. J. Chem. Soc., Perkin Trans. 1, 299–304, https://doi.org/10.1039/P19790000299, 1979.

Chen, H., Yuan, X., Zhang, J., Chen, X., Francisco, J. S., Meng, Y., and Zhang, X.: Simultaneous Reduction and Oxidation of NO_2 on Water Microdroplets Provides Previously Unknown Pathways to the Formation of HONO and HNO_3, J. Am. Chem. Soc., 147, 38500–38507, https://doi.org/10.1021/jacs.5c12051, 2025.

Choi, N. R., Ahn, Y. G., Lee, J. Y., Kim, E., Kim, S., Park, S. M., Song, I. H., and Kim, Y. P.: Winter-time particulate nitrosamines and nitramines in the atmosphere at seoul, South Korea, Atmos. Environ., 237, 117582, https://doi.org/10.1016/j.atmosenv.2020.117582, 2020.

Choi, N. R., Ahn, Y. G., Lee, J. Y., Kim, E., Kim, S., Park, S. M., Song, I. H., Shin, H. J., and Kim, Y. P.: Particulate Nitrosamines and Nitramines in Seoul and Their Major Sources: Primary Emission versus Secondary Formation, Environ. Sci. Technol., 55, 7841–7849, https://doi.org/10.1021/acs.est.1c01503, 2021.

Choi, N. R., Kim, Y. P., Lee, J. Y., Kim, E., Kim, S., and Shin, H. J.: Impact of ozonation on the formation of particulate nitrosodi-methylamine (NDMA) in atmosphere, Chemosphere, 349, 140794, https://doi.org/10.1016/j.chemosphere.2023.140794, 2024.

Choi, N. R., Kim, Y. P., Lee, J. Y., Ahn, Y. G., Kim, E., Kim, S., and Shin, H. J.: Characteristics of the atmospheric behavior of particulate Nitro(so) compounds in the urban atmosphere of Seoul during Spring 2019: Role of the oxides of nitrogen to the formation of Nitro(so) compounds, Atmos. Environ., 358, 121337, https://doi.org/10.1016/j.atmosenv.2025.121337, 2025a.

https://doi.org/10.5194/egusphere-2026-2401
Preprint. Discussion started: 27 May 2026

Choi, N. R., Kim, Y. P., Ahn, Y. G., Lee, J. Y., Kim, E., Kim, S., and Shin, H. J.: Trend and health risk of carcinogenic particulate nitrosamines in the atmosphere in Seoul, South Korea, Atmos. Environ., 356, 121309, https://doi.org/10.1016/j.atmosenv.2025.121309, 2025b.

Da Silva, G.: Formation of Nitrosamines and Alkyldiazohydroxides in the Gas Phase: The CH_3NH + NO Reaction Revisited, Environ. Sci. Technol., 47, 7766–7772, https://doi.org/10.1021/es401591n, 2013.

Deng, X., Ning, A., Liu, L., Bai, F., Yang, J., Li, J., Liu, J., and Zhang, X.: Mechanistic insights into I_2O_5 heterogeneous hydrolysis and its role in iodine aerosol growth in pristine and polluted atmospheres, Atmos. Chem. Phys., 26, 477–488, https://doi.org/10.5194/acp-26-477-2026, 2026.

Evans, D. J. and Holian, B. L.: The Nose–Hoover thermostat, J. Chem. Phys., 83, 4069–4074, https://doi.org/10.1063/1.449071, 1985.

Fang, Y., Li, X., Yuan, C., Li, X., Yuan, X., Zhang, D., Zhang, X., Zhu, C., and Fang, W.: Spontaneous Generation of Alkoxide Radical from Alcohols on Microdroplets Surface, Angewandte Chemie, 137, e202417920, https://doi.org/10.1002/ange.202417920, 2025.

Farren, N. J., Ramírez, N., Lee, J. D., Finessi, E., Lewis, A. C., and Hamilton, J. F.: Estimated Exposure Risks from Carcinogenic Nitrosamines in Urban Airborne Particulate Matter, Environ. Sci. Technol., 49, 9648–9656, https://doi.org/10.1021/acs.est.5b01620, 2015.

Finlayson-Pitts, B. J. and Pitts Jr, J. N.: Chemistry of the Upper and Lower Atmosphere: Theory, Experiments, and Applications. Elsevier., 1999.

Finlayson-Pitts, B. J., Wingen, L. M., Sumner, A. L., Syomin, D., and Ramazan, K. A.: The heterogeneous hydrolysis of NO_2 in laboratory systems and in outdoor and indoor atmospheres: An integrated mechanism, Phys. Chem. Chem. Phys., 5, 223–242, https://doi.org/10.1039/B208564J, 2003.

Frisch, M. J., Trucks, G. W., Schlegel, H. B., Scuseria, G. E., Robb, M. A., Cheeseman, J. R., Scalmani, G., Barone, V., Mennucci, B., Petersson, G. A., Nakatsuji, H., Caricato, M., Li, X., Hratchian, H. P., Izmaylov, A. F., Bloino, J., Zheng, G., Sonnenberg, J. L., Hada, M., Ehara, M., Toyota, K., Fukuda, R., Hasegawa, J., Ishida, M., Nakajima, T., Honda, Y., Kitao, O., Nakai, H., Vreven, T., Montgomery, J. A., Peralta, J. E., Ogliaro, F., Bearpark, M., Heyd, J. J., Brothers, E., Kudin, K. N., Staroverov, V. N., Kobayashi, R., Normand, J., Raghavachari, K., Rendell, A., Burant, J. C., Iyengar, S. S., Tomasi, J., Cossi, M., Rega, N., Millam, J. M., Klene, M., Knox, J. E., Cross, J. B., Bakken, V., Adamo, C., Jaramillo, J., Gomperts, R., Stratmann, R. E., Yazyev, O., Austin, A. J., Cammi, R., Pomelli, C., Ochterski, J. W., Martin, R. L., Morokuma, K., Zakrzewski, V. G., Voth, G. A., Salvador, P., Dannenberg, J. J., Dapprich, S., Daniels, A. D., Farkas, O., Foresman, J. B., Ortiz, J. V., Cioslowski, J. and Fox, D. J.: Gaussian 16, Revision A.03, Gaussian Inc, Wallingford CT, 2016.

Ge, X., Wexler, A. S., and Clegg, S. L.: Atmospheric amines – Part I. A review, Atmos. Environ., 45, 524–546, https://doi.org/10.1016/j.atmosenv.2010.10.012, 2011.

https://doi.org/10.5194/egusphere-2026-2401
Preprint. Discussion started: 27 May 2026

Goedecker, S., Teter, M., and Hutter, J.: Separable dual-space Gaussian pseudopotentials, Phys. Rev. B, 54, 1703–1710, https://doi.org/10.1103/PhysRevB.54.1703, 1996.

Hartwigsen, C.: Relativistic separable dual-space Gaussian pseudopotentials from H to Rn, Phys. Rev. B, 58, 3641–3662, https://doi.org/10.1103/PhysRevB.58.3641, 1998.

Hratchian, H. P. and Schlegel, H. B.: Accurate reaction paths using a Hessian based predictor–corrector integrator, J. Chem. Phys., 120, 9918–9924, https://doi.org/10.1063/1.1724823, 2004.

Hratchian, H. P. and Schlegel, H. B.: Using Hessian Updating To Increase the Efficiency of a Hessian Based Predictor-Corrector Reaction Path Following Method, J. Chem. Theory Comput., 1, 61–69, https://doi.org/10.1021/ct0499783, 2005.

Humphrey, W., Dalke, A., and Schulten, K.: VMD: Visual molecular dynamics, J. Mol. Graph., 14, 33–38, https://doi.org/10.1016/0263-7855(96)00018-5, 1996.

Hutchings, J. W., Ervens, B., Straub, D., and Herckes, P.: N-Nitrosodimethylamine Occurrence, Formation and Cycling in Clouds and Fogs, Environ. Sci. Technol., 44, 8128–8133, https://doi.org/10.1021/es101698q, 2010.

IARC. IARC Monographs on the Evaluation of Carcinogenic Risks to Humans. World Health Organization (WHO), 1978.

Karl, M., Herckes, P., Mitch, W., and da Silva, E. F.: Atmospheric Chemistry-Aqueous phase chemistry. Sintef report, (F23082), 25-05, 2012a.

Karl, M., Herckes, P., Mitch, W., and da Silva, E. F.: SINTEF Materials and Chemistry Process Technology Atmospheric Chemistry-Aqueous phase chemistry Project 257430193: D6 Final report, 2012b.

Kim, J. Y., Kim, Y. P., Yu, X., Yu, J., Wu, Z., Lee, H.-M., Song, M., Jang, K. S., Kim, C., Choi, N. R., and Lee, J. Y.: Concentrations and formation pathways of nitrogen-containing organic compounds in $PM_{2.5}$ from Seoul and Beijing, Environ. Res., 286, 122959, https://doi.org/10.1016/j.envres.2025.122959, 2025.

Kühne, T. D., Iannuzzi, M., Del Ben, M., Rybkin, V. V., Seewald, P., Stein, F., Laino, T., Khaliullin, R. Z., Schütt, O., Schiffmann, F., Golze, D., Wilhelm, J., Chulkov, S., Bani-Hashemian, M. H., Weber, V., Borštnik, U., Taillefumier, M., Jakobovits, A. S., Lazzaro, A., Pabst, H., Müller, T., Schade, R., Guidon, M., Andermatt, S., Holmberg, N., Schenter, G. K., Hehn, A., Bussy, A., Belleflamme, F., Tabacchi, G., Glöß, A., Lass, M., Bethune, I., Mundy, C. J., Plessl, C., Watkins, M., VandeVondele, J., Krack, M., and Hutter, J.: CP2K: An electronic structure and molecular dynamics software package - Quickstep: Efficient and accurate electronic structure calculations, J. Chem. Phys., 152, 194103, https://doi.org/10.1063/5.0007045, 2020.

Lee, C., Yang, W., and Parr, R. G.: Development of the Colle-Salvetti correlation-energy formula into a functional of the electron density, Phys. Rev. B, 37, 785–789, https://doi.org/10.1103/PhysRevB.37.785, 1988.

Li, L., Duan, Z., Li, H., Zhu, C., Henkelman, G., Francisco, J. S., and Zeng, X. C.: Formation of HONO from the NH_3 -promoted hydrolysis of NO_2 dimers in the atmosphere, Proc. Natl. Acad. Sci. U.S.A., 115, 7236–7241, https://doi.org/10.1073/pnas.1807719115, 2018.

https://doi.org/10.5194/egusphere-2026-2401
Preprint. Discussion started: 27 May 2026

Lu, T. and Chen, F.: Multiwfn: A multifunctional wavefunction analyzer, J Comput Chem, 33, 580–592, https://doi.org/10.1002/jcc.22885, 2012.

Ma, J., Qi, Y., Han, Y., Ge, J., Wen, L., Fu, X., Hu, W., Shi, Z., Volmer, D. A., and Fu, P.: Sources and potential health indicators in urban aerosols revealed by gas chromatography-mass spectrometry combined with nitrogen chemiluminescence detector: evidence from a megacity (Tianjin) of China, Atmos. Environ., 358, 121345, https://doi.org/10.1016/j.atmosenv.2025.121345, 2025.

Mai, T. T. H. and Kim, H.: Occurrence of N-nitrosamines in the atmosphere and human health risk: A case study in an urban area of Chuncheon, Gangwon State, South Korea, Environ. Pollut., 349, 123802, https://doi.org/10.1016/j.envpol.2024.123802, 2024.

Marenich, A. V., Cramer, C. J., and Truhlar, D. G.: Universal Solvation Model Based on Solute Electron Density and on a Continuum Model of the Solvent Defined by the Bulk Dielectric Constant and Atomic Surface Tensions, J. Phys. Chem. B, 113, 6378–6396, https://doi.org/10.1021/jp810292n, 2009.

Martins-Costa, M. T. C., Anglada, J. M., Francisco, J. S., and Ruiz-López, M. F.: Theoretical Investigation of the Photoexcited NO_2 +H_2O reaction at the Air–Water Interface and Its Atmospheric Implications, Chem. Eur. J., 25, 13899–13904, https://doi.org/10.1002/chem.201902769, 2019.

Martins-Costa, M. T. C., Anglada, J. M., Francisco, J. S., and Ruiz-López, M. F.: The Aqueous Surface as an Efficient Transient Stop for the Reactivity of Gaseous NO_2 in Liquid Water, J. Am. Chem. Soc., 142, 20937–20941, https://doi.org/10.1021/jacs.0c10364, 2020.

Nielsen, C. J., Herrmann, H., and Weller, C.: Atmospheric chemistry and environmental impact of the use of amines in carbon capture and storage (CCS), Chem. Soc. Rev., 41, 6684, https://doi.org/10.1039/c2cs35059a, 2012a.

Nielsen, C. J., Bossi, R., Bunkan, A. J. C., Dithmer, L., Glasius, M., Hallquist, M., Hansen, A. M. K., Lutz, A., Salo, K., and Maguta, M. M.: Atmospheric Degradation of Amines (ADA): Summary Report from Atmospheric Chemistry Studies of Amines, Nitrosamines, Nitramines and Amides, 2012b.

Ning, A., Zhong, J., Li, L., Li, H., Liu, J., Liu, L., Liang, Y., Li, J., Zhang, X., Francisco, J. S., and He, H.: Chemical Implications of Rapid Reactive Absorption of I_2O_4 at the Air-Water Interface, J. Am. Chem. Soc., 145, 10817–10825, https://doi.org/10.1021/jacs.3c01862, 2023.

Ning, A., Li, J., Du, L., Yang, X., Liu, J., Yang, Z., Zhong, J., Saiz-Lopez, A., Liu, L., Francisco, J. S., and Zhang, X.: Heterogenous Chemistry of I_2O_3 as a Critical Step in Iodine Cycling, J. Am. Chem. Soc., 146, 33229–33238, https://doi.org/10.1021/jacs.4c13060, 2024.

NTP, 2016. In: Program, N. T. (Ed.), 14th Report on Carcinogens (Roc), National Toxicology Program (NTP). US Department of Health and Human Services.

Perdew, J. P. and Wang, Y.: Accurate and simple analytic representation of the electron-gas correlation energy, Phys. Rev. B, 45, 13244–13249, https://doi.org/10.1103/PhysRevB.45.13244, 1992.

https://doi.org/10.5194/egusphere-2026-2401
Preprint. Discussion started: 27 May 2026

Seinfeld, J. H. and Pandis, S. N.: Atmospheric Chemistry and Physics: From Air Pollution to Climate Change; John Wiley & Sons, 2016.

Song, Z., Zhu, C., Gong, K., Wang, R., Zhang, J., Zhao, S., Li, Z., Zhang, X., and Xie, J.: Deciphering the Microdroplet Acceleration Factors of Aza-Michael Addition Reactions, J. Am. Chem. Soc., 146, 10963–10972, https://doi.org/10.1021/jacs.4c02312, 2024.

Wang, H. and Agmon, N.: Reinvestigation of the Infrared Spectrum of the Gas-Phase Protonated Water Tetramer, J. Phys. Chem. A, 121, 3056–3070, https://doi.org/10.1021/acs.jpca.7b01856, 2017.

Wang, J., Zhou, X., Hua, Z., Jiang, N., and He, X.: Concentration level, health risk assessment and source apportionment of nitrosamines in $PM_{2.5}$ in Urumqi during winter time, Atmos. Pollut. Res., 14, 101756, https://doi.org/10.1016/j.apr.2023.101756, 2023.

Zhang, Q. and Anastasio, C.: Chemistry of fog waters in California's Central Valley—Part 3: concentrations and speciation of organic and inorganic nitrogen, Atmos. Environ., 35 (32), 5629–5643, https://doi.org/10.1016/S1352-2310(01)00337-5, 2001.